

GT2009-59567

FILM COOLING EFFECTIVENESS AND HEAT TRANSFER NEAR DEPOSIT-LADEN FILM HOLES

Scott Lewis, Brett Barker, Jeffrey P. Bons

Department of Aerospace Engineering, The Ohio State University, Columbus, OH, 43235

Weiguo Ai, Thomas H. Fletcher

Department of Chemical Engineering, Brigham Young University, Provo, UT, 84602

ABSTRACT

Experiments were conducted to determine the impact of synfuel deposits on film cooling effectiveness and heat transfer. Scaled up models were made of synfuel deposits formed on film-cooled turbine blade coupons exposed to accelerated deposition. Three distinct deposition patterns were modeled: a large deposition pattern (max deposit peak \cong 2 hole diameters) located exclusively upstream of the holes, a large deposition pattern (max deposit peak \cong 1.25 hole diameters) extending downstream between the cooling holes, and a small deposition pattern (max deposit peak \cong 0.75 hole diameter) also extending downstream between the cooling holes. The models featured cylindrical holes inclined at 30 degrees to the surface and aligned with the primary flow direction. The spacing of the holes were 3, 3.35, and 4.5 hole diameters respectively. Flat models with the same film cooling hole geometry and spacing were used for comparison. The models were tested using blowing ratios of 0.5-2 with a turbulent approach boundary layer and 0.5% freestream turbulence. The density ratio was approximately 1.1 and the primary flow Reynolds number at the film cooling row location was 300,000. An infrared camera was used to obtain the film cooling effectiveness from steady state tests and surface convective heat transfer coefficients using transient tests. The model with upstream deposition caused the primary flow to lift off the surface over the roughness peaks and allowed the coolant to stay attached to the model. Increasing the blowing ratio from 0.5 to 2 only expanded the region that the coolant could reach and improved the cooling effectiveness. Though the heat transfer coefficient also increased at high blowing ratios, the net heat flux ratio was still less than unity, indicating film cooling benefit. For the two models with deposition between the cooling holes, the free stream air was forced into the valleys in line with the coolant holes and degraded area-averaged coolant performance at lower blowing ratios. It is concluded that the film cooling effectiveness is highest when deposition is limited to upstream of the cooling holes. When accounting for the insulating effect of the deposits between the film holes, even the panels with

deposits downstream of the film holes can yield a net decrease in heat flux for some cases. [*Keywords:* deposition, roughness, film cooling]

NOMENCLATURE

DR = density ratio (ρ_c/ρ_∞)

L = wind tunnel length from bleed to film cooling holes (0.57m)

M = blowing ratio ($\rho_c U_c/\rho_\infty U_\infty$)

Ma = Mach number

Ra = centerline averaged roughness [mm]

Re_c = chord Reynolds number $U_{ex}c/\nu$

Re_d = hole diameter Reynolds number $U_\infty d/\nu$

Re_L = flow Reynolds number $U_\infty L/\nu$

Rq = rms roughness [mm]

Rt = maximum peak-to-valley roughness [mm]

S = surface area

St = Stanton number ($h/\rho_c p U_\infty$)

T = flow temperature [C]

U = velocity

c_f = skin friction coefficient

d = film hole diameter: 1mm (coupon) or 17.5mm (model)

h = convective heat transfer coefficient

k = thermal conductivity

q = heat flux

s = spacing between film holes

t = time or deposit thickness

x = surface dimension parallel to the gas stream (x=0 at downstream end of film hole)

y = surface dimension perpendicular to the gas stream

z = vertical distance perpendicular to the wall

Φ = overall cooling effectiveness

α = thermal diffusivity

κ = thermal conductivity

η = adiabatic film cooling effectiveness $(T_\infty - T_w)/(T_\infty - T_c)$

ν = kinematic viscosity

ρ = density

subscripts

R = deposit roughness panel

S = smooth panel

c = chord

eff = effective (see Eq. [4])

f = film (average of freestream and wall value)

m = time indexing variable in Eq. [2]

n = time step in Eq. [2]

o = no cooling (M=0) baseline

p = planform

w = wall or surface

wt = wetted

∞ = freestream

INTRODUCTION

Turbine blades routinely operate in a severe environment of hot combustion gases above the metallurgical limits of the blade. This is made possible through a combination of intricate cooling systems and thermal barrier coatings. There is always a tradeoff between operating the combustor as hot as possible in order to achieve high thermal efficiencies, while low enough to ensure long life of the turbine components. Turbine blades are cooled using relatively cool compressor air which bypasses the combustion section (thus reducing the net power output). A considerable amount of engineering goes into optimizing the cooling system so that the turbine components are sufficiently cooled while the use of compressor air is minimized to achieve optimum cycle efficiencies.

Turbine blades are cooled internally with serpentine cooling passages as well as externally with film cooling. Film cooling is typically characterized by the coolant to freestream mass flux ratio or blowing ratio (M) as well as the coolant to freestream density ratio (DR). Typical blowing ratios on turbine blades range from 0.5 to 2.0, while density ratios range from 1.5 to 2.0. In general the coolant performance increases with increased blowing ratio, until blow off occurs. Blow off refers to when the coolant jet leaves the turbine surface and enters into the mainstream gas.

Synthetic fuels also known as synfuels are a liquid or gaseous fuel derived especially from a fossil fuel that is a solid, such as coal, or part of a solid, like tar sand or oil shale. The use of synfuels in land-based industrial gas turbines is of interest as turbine operators seek greater fuel flexibility. Natural gas has been the primary fuel for gas turbines commissioned in the last two decades, and the industrial turbine industry would like other options as the cost of natural gas rises. Synfuels, as opposed to natural gas, are dirty fuels and produce a considerable amount of particulate during the combustion process. This particulate in the combustion gas can cause either erosion, or deposition on the turbine blades depending on the temperature of the particulate. If the particulate is below its softening temperature, then erosion will likely occur. While if the particulate is above its softening temperature, the particulate may stick to the blade and deposition is more likely to occur [1,2]. Deposition changes the shape and aerodynamic performance of the turbine blade [3,4] and can block critical film cooling holes [5]. Deposition also increases the surface roughness [6], resulting in increased heat transfer to the blade surface.

A number of studies have explored the effects of roughness on film cooling performance [7-11]. In general researchers have found that at low blowing ratios roughness reduces the film effectiveness (η) while at high blowing ratios, roughness can actually improve η by limiting jet lift-off from the surface. Surface roughness degrades performance at low blowing ratios through two mechanisms. First, rough surfaces produce thicker boundary layers and thus lower near-wall velocities compared to smooth surfaces. This produces a higher “effective” blowing ratio for the roughness-thickened boundary layer which can lead to jet lift-off at lower values of M. Second, roughness generates significant near wall turbulence that dissipates coolant more rapidly. Film cooling effectiveness alone does not capture the full effect of roughness on film cooling since roughness also enhances surface heat transfer. When the combined effects on film cooling effectiveness and heat transfer are properly accounted for, the result can be a 30-70% increase in surface heat flux with roughness [8] (compared to a smooth surface).

Considerable attention has also been given to the damaging effect of deposit-like flowpath obstructions on film effectiveness. Demling and Bogard [12] positioned obstructions both upstream and downstream of a film cooling hole, as well as in the hole itself. In general, these obstructions produced drastic degradation of the film cooling effectiveness. Obstructions at the upstream location showed greater degradation than those at the downstream location. For example, obstructions with a height of 0.25d located directly upstream of the film hole produced a 25% to 80% drop in η for $M > 0.7$ and degradation increased with increasing blowing ratio. Downstream obstructions had a small effect on film cooling performance at mid and high blowing ratios of $M = 0.7$ and 1.2. Somawardhana and Bogard [13] also studied the effects of surface roughness and near-hole obstructions on film cooling effectiveness. Obstruction height had the largest effect, with obstructions 0.5d in height causing as large as 40% reduction in η at low blowing ratios and a 30% reduction at high blowing ratios. The shape of the obstruction had a very small effect on heat transfer. Sundaram and Thole [14] studied the effects of surface deposition, hole blockage, and TBC spallation on vane endwall film-cooling. Near hole depositions were studied with varying deposit heights. For smaller deposit height (0.5D) the overall film-cooling effectiveness was actually enhanced by 25%. With an increase in deposit height to 1.2D, blow off occurred and η dropped substantially.

The objective of this study is to analyze the heat transfer effects of deposition on film cooling performance using as close to an actual synfuel deposition topography as possible. This study is different from other studies in that actual deposition topography is incorporated into the film cooling model. All previous film cooling heat transfer studies have used non-deposit shapes (e.g. cubes, cones, or cylinders) to simulate deposit roughness.

ROUGHNESS MODELS

The Turbine Accelerated Deposition Facility (TADF) located at BYU was employed to generate the film cooling deposits used for the scaled models in this study. The facility replicates the deposition chemistry and topography of several months of turbine operation in a one hour accelerated test. The facility generates deposits on actual turbine material systems

while matching the gas temperature (1180C), freestream Mach number (0.2), particulate size (4-16 μ m), film cooling blowing ratio ($0 < M < 4$), and density ratio (1.8-2.3) of a typical turbine environment. A detailed description of the facility is provided by Jensen et al [15], who also verified that the deposition chemistry and topology produced from the accelerated facility match those found on deposited industrial turbine blades. For the present study, the natural gas burning combustor was seeded with subbituminous coal fly ash obtained from a power plant. The ash composition is available in Crosby et al [16]. The coal ash was ground to mass mean particle diameters of 4 or 16 μ m.

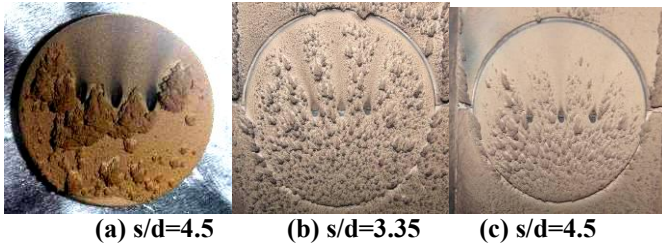


Figure 1: After deposition photographs of the three turbine blade coupons.

The 2.5cm diameter nickel-based superalloy turbine coupons used in the TADF were donated from industry. Digital images of each coupon taken immediately after the deposition testing are shown in Fig. 1. Test data for each case are included in Table 1. The individual film cooling hole geometries are identical for all cases: 1mm diameter, 30° incline, cylindrical holes, aligned with flow direction, and length = 6 hole diameters. Approximately the same amount of coal ash particulate (15g) was used in each 1-hour deposition test, though the fraction of particulate that accumulated on the coupons varied with blowing ratio and surface type.

Table 1: Data for deposition coupons shown in Fig. 1

Coupon	M	DR	s/d coupon	s/d scale model
1	4	1.72	4.5	3
2	1	1.83	3.35	3.35
3	2	2.1	4.5	4.5

Following the deposition test, a Helmel Microstar Coordinate Measuring Machine (CMM) was used to optically scan the test surface. The scanned surface was exported as xyz point cloud data for further manipulation in Matlab™. For Coupon #1, the scan was trimmed to only include the area within $y = \pm 1.5d$ of the middle film cooling hole. This middle section was then mirrored repeatedly in the cross-stream direction to form the desired wind tunnel model with six film cooling holes. Thus the scaled model of this coupon had a hole spacing to diameter ratio of 3. The middle section was chosen because the flow conditions better approximate those of a film cooling hole in a continuous row. Also, because the large deposits just upstream of the film holes dominated the roughness topology by at least a factor of 4-5 in size, all of the smaller deposit features were neglected when fabricating this model.

For the second two coupons, the scanned data were trimmed to include the middle hole and up to half of the adjacent holes ($y = \pm 3.35d$ and $y = \pm 4.5d$ respectively). The scans were mirrored about the centerline of the adjacent holes to provide 6 complete film cooling holes for the second scan and 5 holes for the third scan. Thus, Coupons 2 & 3 preserve the original s/d spacing of the TADF test articles. For these two models, the point cloud data was adjusted to align the downstream deposition between the film cooling holes with the freestream direction in the wind tunnel.

The 32cm (x) by 38cm (y) by 2cm (z) film cooling wind tunnel models were produced using stereolithography. Figure 2 shows photographs of the 3 models. A scaling factor of 17.5 was selected to provide adequate spatial resolution for surface imaging while also matching Re_L and Re_d with typical values on actual turbine hardware. A typical turbine vane exit Reynolds number based on chord (Re_c) is $1e^6$. With a streamwise tunnel location (L) for the film row of 0.57m and 8.5 m/s freestream velocity in the wind tunnel, Re_L is approximately $3e^5$. This indicates a film row location of roughly 30% of the total vane chord. The equivalent “chord” length in the wind tunnel would then be approximately 1.9m. Thus, the ratio of model hole size (17.5mm) to model chord length is 108. This matches the chord to film hole diameter ratio for an industrial gas turbine blade with 1mm holes and a 10.8 cm chord length. The Reynolds number based on hole diameter is 9,200.

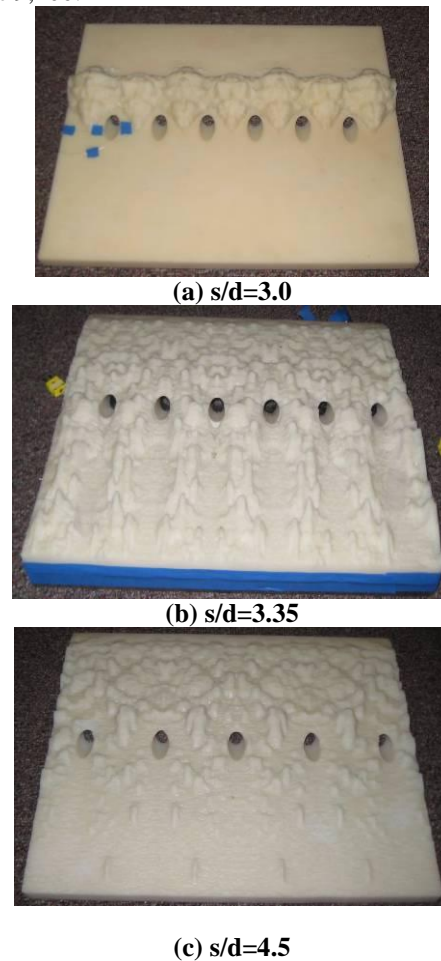


Figure 2: Digital images of the stereolithography models corresponding to the deposit patterns in Fig. 1.

Companion models without roughness were also fabricated to provide a control. The film hole length to diameter ratio is five for the first smooth model and four for the second and third. The length to diameter ratios are slightly larger for the models with deposits since they have additional material built up near the hole exit. The stereolithography plastic is Somos 18420, a low viscosity liquid photopolymer with a white, opaque appearance. The thermal properties of this material are: specific heat = $1325 \pm 3\%$ J/kg-K, density = $1194 \pm 2\%$ kg/m³, and thermal diffusivity = $0.00146 \pm 6\%$ cm²/sec. The vertical resolution of the stereolithography process was 0.15mm.

The three-dimensional surface files were used to produce roughness statistics for various regions of the 3 deposit panels. The statistics of most interest for this study were the centerline averaged roughness, R_a , the rms roughness, R_q , and the peak roughness height, R_t , all normalized by the film hole diameter (17.5mm).

The $s/d=3$ panel has a maximum deposit height of 2.1d between the film holes, dropping down to 1.5d directly upstream of the hole. The deposits are only located immediately upstream of the row of holes as depicted in Fig. 2.

The $s/d=3.35$ panel has $R_a=0.09d$, $R_q=0.12d$, and $R_t=0.83d$ upstream of holes. Downstream of the holes, deposits accumulated primarily between the holes, creating a “furrowed” deposit patterns that bears striking resemblance to deposit features noted on actual turbine hardware as reported by Bons et al. [6]. Roughness measurements downstream and between holes were $R_a=0.24d$, $R_q=0.29d$, and $R_t=1.2d$ compared with $R_a=0.1d$, $R_q=0.13d$, and $R_t=0.51d$ directly downstream from the holes.

The $s/d=4.5$ panel shows a similar pattern to $s/d=3.35$ panel, but with lower roughness levels throughout due to the increased coolant blowing ratio used in the TADF deposition test: upstream ($R_a=0.13d$, $R_q=0.15d$, and $R_t=0.77d$), downstream between holes ($R_a=0.06d$, $R_q=0.08d$, and $R_t=0.5d$), and downstream of holes ($R_a=0.02d$, $R_q=0.02d$, and $R_t=0.21d$).

EXPERIMENTAL FACILITY

An open loop wind tunnel powered by a blower was used for the heat transfer measurements in this study (Fig. 3). An electric duct heater is located after the blower and can be used to vary the freestream flow temperature from 20° to 60°C. The flow then passes through a 0.6 m diameter conditioning plenum before reaching the square test section. The conditioning plenum includes one layer of perforated aluminum plate, 7.6 cm of honeycomb straightener, followed by five layers of fine screen. A circular-to-square foam nozzle transitions the flow from the plenum to the 0.38 m by 0.38 m square test section. With this conditioning, 2D flow uniformity of $\pm 0.4\%$ in velocity and $\pm 1^\circ\text{C}$ is obtained over the center 0.18 m of the test section span. The freestream turbulence level in the wind tunnel is 0.5%.

At 1.52 m from the plenum exit a knife-edge boundary layer suction bleed is used to pull off the bottom 2.7 cm from the growing boundary layer. A 1.6 mm diameter boundary layer trip was placed 2.5cm downstream of the knife edge which yielded a 17mm thick turbulent boundary layer (shape factor = 1.4) at the film cooling hole location with the smooth film cooling model. The film cooling holes are located .57 m. from the knife edge boundary layer suction point and .18 m. from the

upstream edge of the stereolithography model. For the roughness panels the flow in the tunnel experiences a transition from a smooth to rough wall condition at the leading edge of the panel. Several studies have shown [17-18] that this smooth to rough transition results in an initial overshoot in c_f and St followed by a rapid adjustment to the fully-developed rough-wall values within 3-4 boundary layer thicknesses. To mitigate the effect of this transition region, the heat transfer data were taken on the downstream half of the roughness section (beyond the expected adjustment length of approximately 8 cm).

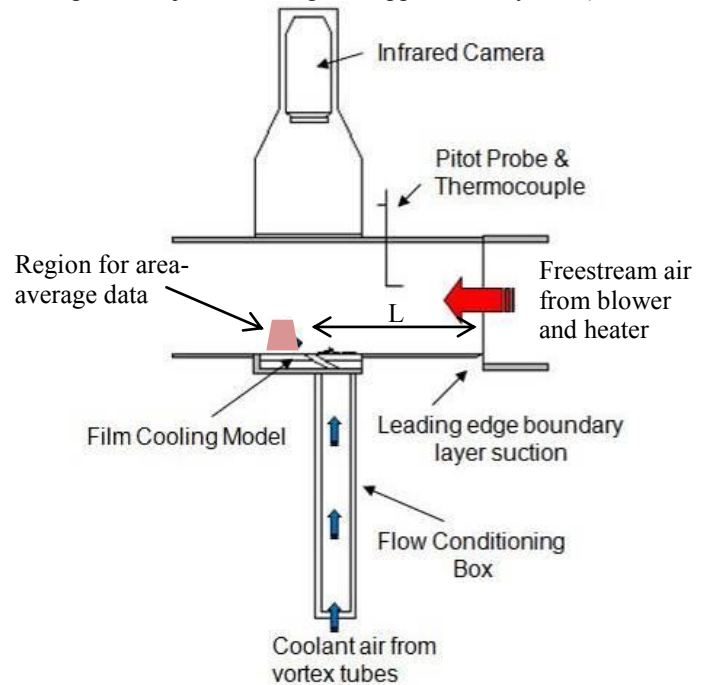


Figure 3: Film cooling wind tunnel test section diagram.

Flow velocity was measured using a pitot-static probe with a co-located flow thermocouple with 0.13 mm bead diameter. The two instruments are positioned at midspan just outside the boundary layer and upstream of the film cooling panels. Uncertainty in the velocity measurement was within $\pm 1.5\%$ at flow rates of interest.

A coolant flow conditioning box was built to supply the film cooling holes. The box is lined with a 2cm thick layer of low thermal conductivity foam to reduce thermal losses. The box conditions the flow using two sheets of fine screen, which help to provide a straight and uniform flow to the film cooling holes. The centerline velocity of the coolant at each of the film cooling holes was within 0.5 m/s or 6% at $M=1$. Temperature uniformity was found to be within 0.5°C at the lowest possible coolant temperature of -13°C. The coolant air is supplied by a high pressure air line and cooled using three vortex (Ranque-Hilsch) tubes aligned in parallel. The vortex tube configuration is capable of supplying 60 cfm with temperatures ranging from room temperature down to -15°C (maximum temperature drop of 36°C). The maximum blowing ratio was $M=2$. Data were acquired at $M = 0, 0.5, 1.0,$ and 2.0 for all three models. Additional data were acquired at $M=1.5$ for the $s/d=3$ model in order to further elucidate non-monotonic trends in the results. An Electrophysics Silver 420 shortwave infrared camera was used for this study. The camera has a 320 x 256 pixel Indium Antimonide (InSb) detector with a 20° x 16° field of view and a

3.6 to 5.1 μm spectral range. The camera has a measurement accuracy of $\pm 2\%$ or $\pm 2^\circ\text{C}$ and a maximum frame rate of 100Hz. The model emissivity was measured to be 0.9. The camera was focused on a 29.5cm (x) by 23.5cm (y) field of view centered on the film cooling holes.

The goal of this study is to understand the heat transfer effects of synfuel deposition on film cooling performance. A common way to quantify the heat transfer effects of film cooling is to compare the local heat flux with film cooling (q) to the heat flux without film cooling (q_0) [Eq. (1)]. The variables h and h_0 are the local convective heat transfer coefficients with and without film cooling, respectively. The heat transfer coefficient with film cooling, h , is typically higher than the heat transfer coefficient without film cooling, h_0 . Note that in the presence of film cooling the driving temperature for convection in Eq. (1) is the film temperature, T_f , rather than the gas freestream temperature, T_∞ . The heat flux ratio can be rewritten using the definition for film effectiveness, η , as shown. Equation (1) can be used to determine the net benefit of film cooling since a value less than unity indicates a net cooling benefit. Typical values of T_∞ , T_c , and T_w for turbines yield an overall cooling effectiveness, $\Phi = 0.6$ [19]

$$\frac{q}{q_0} = \frac{h}{h_0} \frac{(T_f - T_w)}{(T_\infty - T_w)} = \frac{h}{h_0} \left\{ 1 - \eta \frac{(T_\infty - T_c)}{(T_\infty - T_w)} \right\} = \frac{h}{h_0} \left\{ 1 - \frac{\eta}{\Phi} \right\} \quad (1)$$

In this study, two separate tests were used to obtain the desired heat flux ratio. A steady state test was performed to obtain the film cooling effectiveness, η , and a transient test was performed to obtain the convective heat transfer coefficient, h . The two tests were performed at different coolant and freestream temperatures, but correlated by matching the blowing ratio, M , and density ratio, DR . For the film cooling effectiveness tests, the freestream air temperature was 25°C , and the coolant source temperature was adjusted to obtain the desired density ratio (1.1). The coolant temperature was measured with a thermocouple at the exit of the film cooling holes. The waiting time for the model to come to steady state was typically over 1 hour. Since the model is not an adiabatic surface, conduction losses result in slightly lower surface temperatures than would be obtained with a truly adiabatic surface (radiation losses are negligible). The conduction loss was corrected by subtracting a no-cooling effectiveness case from the measurement obtained with coolant, similar to the procedure outlined by Rutledge et al. [8]. A thermocouple sandwiched beneath the model verified comparable conduction losses in both the coolant “on” and “off” cases.

The uncertainty in the η measurement arises from the IR camera uncertainty and the thermocouple measurement uncertainty. While the accuracy of the IR camera is reported by the manufacturer as $\pm 2^\circ\text{C}$, this is a bias error. The uncertainty due to precision error is an order of magnitude lower. The thermocouple measurement uncertainty was $\pm 1^\circ\text{C}$. The uncertainty for a typical value of $\eta=0.2$ is ± 0.02 .

The convective heat transfer coefficient was obtained using a transient method. The film cooling model was placed inside the wind tunnel with low thermal conductivity foam sealing off the upstream and downstream passageways. This allowed the plastic model to come to a uniform temperature after a period of at least 3 hours. Once the waiting time had passed, the

freestream air (heated to around 48°C) was diverted over the model at the same instant that room temperature coolant flow was initiated. The three minute transient tests were recorded with an infrared camera which provided temperature maps on the surface. The flow velocities and temperatures were also recorded.

The convective heat transfer coefficient was determined from these temperature data using the 1D method of Schultz and Jones [20]. This technique uses Duhamel’s superposition method to calculate the surface heat flux given the surface temperature history. It assumes the panels are a semi-infinite solid at uniform temperature at time $t = 0$. The heat transfer coefficient (h) at the n^{th} time step is then calculated using the expression from Schultz and Jones.

$$h_n = \frac{1}{T_\infty - T_{wn}} \left[\frac{2\kappa}{\sqrt{\pi\alpha}} \sum_{m=1}^n \frac{T_{wm} - T_{wm-1}}{\sqrt{t_n - t_m} + \sqrt{t_n - t_{m-1}}} \right] \quad (2)$$

This transient testing methodology is described in greater detail in Bons [4]. Radiative heat flux from the test plate to the surrounding tunnel walls was always less than 1% of the calculated convective heat flux.

During testing the 20 mm thick plastic film cooling panels were mounted on a second 20 mm thick smooth acrylic panel with the same material properties. A thermocouple sandwiched between the 2 panels indicated no change in temperature during the first four minutes for the typical test case. This confirmed the use of the semi-infinite conduction assumption in the data processing. Also, it was discovered that the infrared measurement is sensitive to the temperature of the surfaces surrounding the roughness panels. This occurs because some of the radiation that is incident on the camera originates from the wind tunnel enclosure and is reflected off the film cooling panel. The magnitude of this component of radiation changes as a function of the tunnel wall temperature. The Electrophysics software accounts for this by allowing the user to specify the ambient enclosure temperature. Since the heat transfer test was transient, this input was adjusted in post-processing to track the tunnel wall temperature as a function of time. The average h values presented in this report were calculated by averaging the initial 180 seconds of the plate’s transient response. The smooth plate St value was found to be within 5% of a standard correlation. Repeatability was within $\pm 4\%$ and bias uncertainty was estimated at ± 0.00015 for the smooth plate measurement of $St_0 = 0.00253$ at $Re_L = 3e^5$.

Because the Schultz and Jones analysis assumes a 1D conduction path (in the z direction only), errors are induced in the transient heat transfer coefficient calculation from three sources: local surface temperature gradients in the x and y directions, local variations in surface topology due to roughness, and three-dimensional solid property variations (due to the voids created by the film holes). The first two error sources are addressed at length in Bons [21,22]. Temperature gradients on an otherwise flat surface do not change the area-averaged h calculation from the 1D transient conduction method. However, surface roughness does result in an underestimate of the area-averaged heat load to the surface (when normalized by the planform area). In the reference cited [21], a wetted-to-planform surface area ratio (S_{w}/S_p) of 1.063 yielded an underestimate of 3% in area-averaged h . The S_{w}/S_p ratios for the $s/d=4.5$ & 3.35 models are 1.12 and 1.30 respectively in the region of interest. If the correction is

assumed to be linear with S_{wt}/S_p , the area averaged h values should be adjusted upward by 6.5% and 18% for the $s/d = 4.5$ and 3.35 roughness topologies respectively. This correction was not assessed to the data presented in this paper since the linear relationship has not been verified. Near hole 3D conduction effects are a final source of error, primarily in the region very near the film hole. Accordingly, area-averages are only reported for $x/d > 0.5$. These transient 3D conduction corrections do not affect the η measurement since it was steady-state.

RESULTS AND DISCUSSION

The selection of three film cooling models with different hole spacing to diameter ratios (s/d) permits the evaluation of the effect of hole spacing on film effectiveness, heat transfer, and net heat load without the presence of deposits. Figure 4 shows the spanwise average film effectiveness at $x/d=5$ with a comparison to Brown and Saluja [23] who studied a much broader range ($3 < s/d < 4.5$ vs. $2.67 < s/d < 8$ respectively). As might be expected, there is a significant fall off in spanwise average effectiveness as the spacing is increased due to the lower surface coverage of the coolant film.

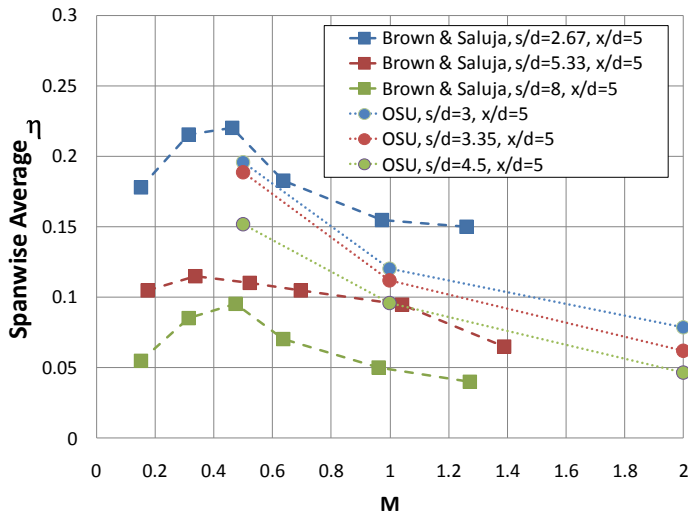


Figure 4: Spanwise-averaged film effectiveness at $x/d = 5$ for present study vs. Brown and Saluja [23]. Smooth panels only.

Similar trends are evident when the comparison is made using the area average film effectiveness over the entire downstream region ($0.5 < x/d < 7$). This trend is shown in Fig. 5 which also includes the heat transfer coefficient and heat flux ratios for the smooth panels only. Both the heat transfer coefficient and heat flux are normalized by the $M=0$ smooth baseline case (h_{so} and q_{so} respectively). It should be noted that the holes were not covered for the $M=0$ case due to the difficulty of taping over the film holes with adjacent deposits on the non-smooth models. Averages are made over two holes, including the centermost hole in the wind tunnel. As the hole spacing is increased from 3 to 4.5, the elevated convective heat transfer associated with the coolant injection becomes less prominent since it occupies a smaller fraction of the area used for averaging. Thus, when the heat flux ratio is calculated (Eq. 1), the decreased heat transfer coefficient ratio overcomes the

lower film effectiveness of the greater spacing and makes the cooling more effective at high blowing ratios when the h_s/h_{so} values exceed unity by 20-40%.

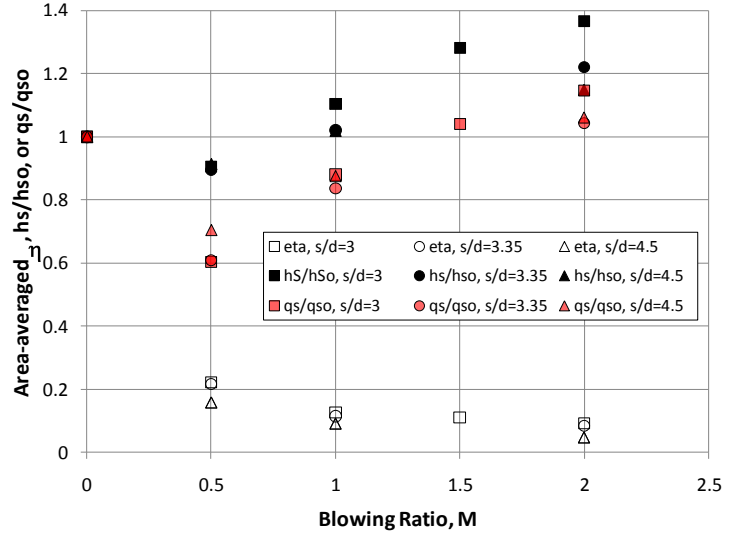


Figure 5: Area-averaged film effectiveness, heat transfer coefficient ratio, and heat flux ratio vs. M ($0.5 < x/d < 7$). Smooth panels only.

With deposits, the trends in Fig. 5 are altered significantly. Figure 6 contains film effectiveness contour maps for smooth and deposit panels at $M=1$. Perhaps the most obvious alteration is that the $s/d=3$ deposit panel has higher η levels than any of the other panels (including smooth). The likely reason has to do with the size and location of the deposit structures. For the $s/d=3.35$ and 4.5 panels, the roughness is distributed upstream and downstream (primarily between the film holes). For these panels, the increased mixing due to upstream roughness actually improves the near hole centerline effectiveness values probably due to the mechanism cited earlier; namely upstream roughness increases the boundary layer thickness and lowers the “effective” blowing ratio thus reducing the near-hole effect of jet blow-off. The coolant also appears to spread more rapidly in the lateral direction due to the heightened boundary layer mixing. These effects are more pronounced for the $s/d=3.35$ deposit panel due to the larger roughness structures compared to the $s/d=4.5$ panel. The $s/d=3$ deposit panel experiences a very different deposit effect. Since the deposit is both large (height $\cong 2d$) and exclusively upstream of the hole, it creates an effective “backward facing step” for the incoming boundary layer with an associated separation cavity. This cavity is subsequently filled with coolant, providing excellent spanwise coverage.

Figure 7 summarizes these results over the full range of blowing ratio. At the lowest blowing ratio, the deposits reduce the area-averaged effectiveness in all cases. However, as blowing ratio is increased, the $s/d=3.35$ & 4.5 panels with distributed deposits show little if any effect on η . By comparison, the η levels for upstream roughness increase monotonically with M . This result is distinctly opposite that reported by Demling and Bogard [12] who reported a universal drop in effectiveness with upstream obstructions. The key difference here is that the TADF generated deposits do not form in the manner tested by Demling and Bogard who used

isolated deposits with spanwise extent approximately equal to the film hole diameter. As evident in Fig. 1, the TADF coupon experienced upstream deposition across the entire hole spacing, with the largest upstream deposits forming between the holes. This deposit topology produces an effect similar to the upstream ramp studied by Na and Shih [24] who reported increases in effectiveness of 2-3 times. It should be noted that in a follow-on study, Somawardhana and Bogard [13] did explore the effect of offsetting the upstream obstructions in the spanwise direction and found increased area-average effectiveness for obstruction heights up to $0.75d$. This configuration more closely resembles the $s/d=3$ case studied here, with the largest upstream deposits concentrated between the film holes.

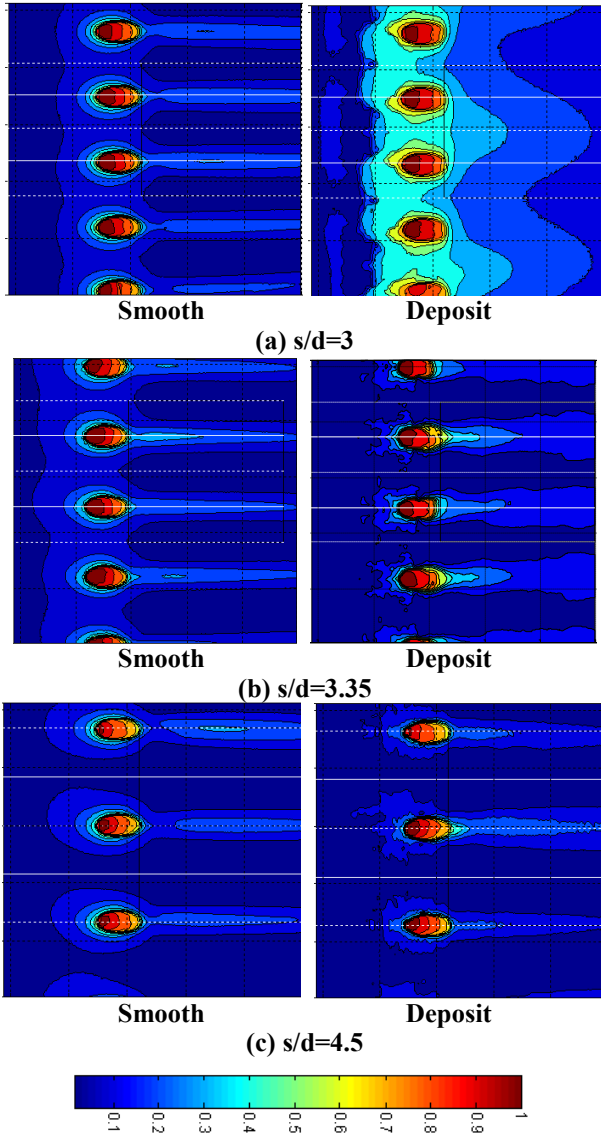


Figure 6: Film effectiveness contour maps for smooth and deposit panels at $M=1$. (Flow is left to right)

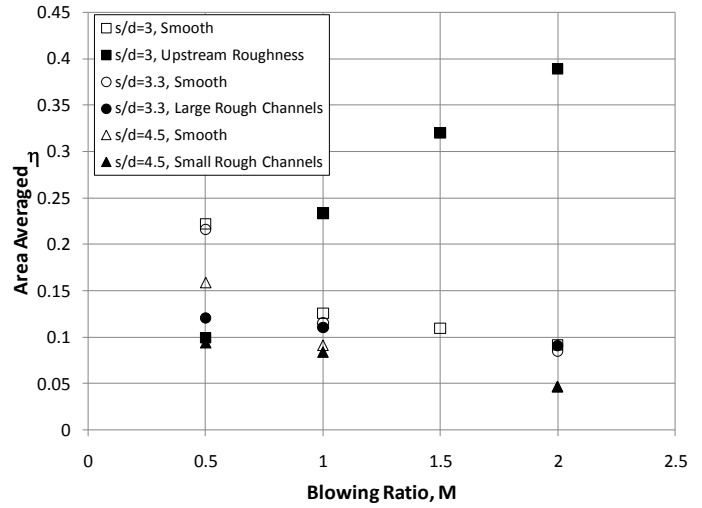


Figure 7: Area-averaged film effectiveness vs. M ($0.5 < x/d < 7$). Both smooth and deposit panels.

As mentioned earlier, the film effectiveness parameter does not capture all of the effects of surface deposits on film cooling. Figure 8 shows the effect of deposits on convective heat transfer coefficient ratio for all three deposit panels. The ratio is made using the $M=0$ case for each panel (e.g. the $M=2$, $s/d=3$ deposit panel h_R is normalized by the $M=0$, $s/d=3$ deposit panel h_{R0} value). For almost all of the cases studied, film cooling increases the convective heat transfer. The increase is greater for the rough panels compared to the smooth and increases with increased blowing ratio. Again, the $s/d=3$ panel presents a unique case worth investigating. At low blowing ratios, this panel with only upstream deposits actually produces a decrease in heat transfer coefficient up to $M=1$. The coolant fills the void downstream of the deposit “ramp” and produces a calming effect. This beneficial effect is lost at higher blowing ratios ($M \geq 1.5$) when the jet momentum is sufficient to penetrate the separated shear layer over the deposit “ramp”. In this case, enhanced mixing produces a dramatic rise in heat transfer coefficient for the region encompassed in the area-average. This loss of “upstream ramp” benefit at high M was also noted in the study of Barigozzi et al. [25] who attempted to experimentally verify the computational results of Na and Shih [24].

Another instructive comparison that can be made with the data in Fig. 8 is to ratio the deposit panel h_R to the smooth panel h_S at the same value of M . This is plotted in Fig. 9. While Fig. 8 provides information on what happens when film cooling is increased on a deposit-laden (or smooth) panel, Fig. 9 provides a perspective on what happens to film cooling at a fixed M when deposits begin to form around the film hole. Corroborating the result from Fig. 8, only in the case of the upstream deposit panel (at low M) is the deposit actually beneficial in lowering the heat transfer coefficient. It is expected that if the area-average were extended further downstream beyond $x/d=7$, even these cases would likely show $h_R/h_S > 1$ due to the reattaching shear layer and heightened mixing.

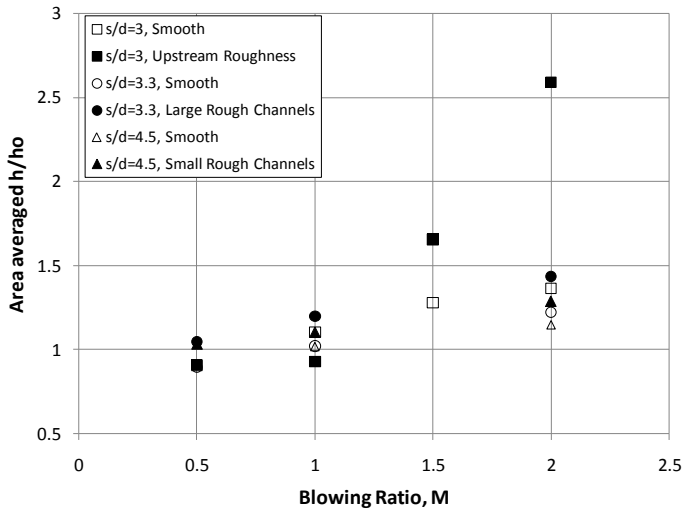


Figure 8: Area-averaged convective heat transfer ratio vs. M ($0.5 < x/d < 7$). Both smooth and deposit panels.

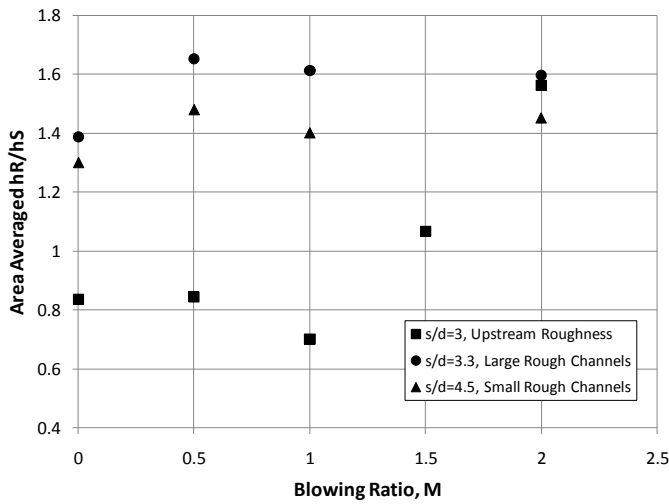


Figure 9: Area-averaged rough-to-smooth convective heat transfer ratio vs. M ($0.5 < x/d < 7$). Comparison at constant blowing ratio.

The full effect of deposits on film cooling performance is embodied in the heat flux ratio defined earlier [Eq. (1)]. Heat flux ratios less than unity represent a net cooling benefit while values greater than unity suggest that the heat load would be less if film cooling holes were eliminated altogether. Figure 10 contains the heat flux ratio for both the smooth and deposit panels. Again, the ratio is made using the $M=0$ case for each panel (e.g. q_R is normalized by q_{R0} and q_S is normalized by q_{S0}). As hoped, all but the highest blowing ratios show a net benefit for film cooling. The smooth panel results are similar to those reported elsewhere [19]. Surprisingly, for the upstream deposit case, the increased film effectiveness (Fig. 7) dominates the heightened convective heat transfer (Fig. 8) to yield a reduced heat flux over all of the M values tested. Based on the apparent trend in the data, this unexpected benefit may disappear at blowing ratios greater than two. Also, as noted earlier, the perceived benefit may be substantially reduced if the area-average is extended beyond $x/d=7$.

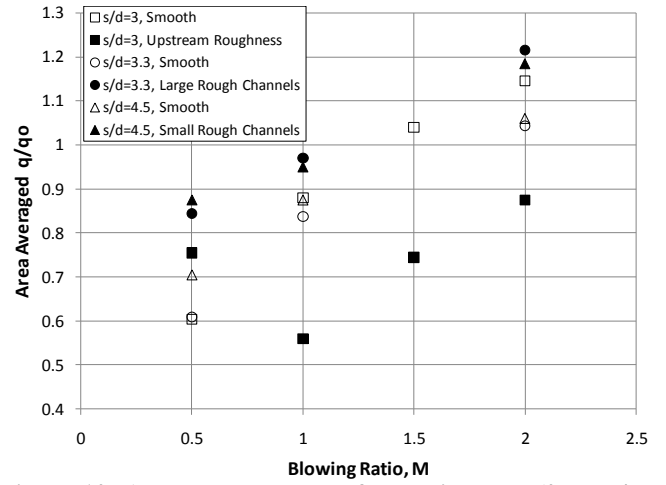


Figure 10: Area-averaged heat flux ratio vs. M ($0.5 < x/d < 7$). Both smooth and deposit panels.

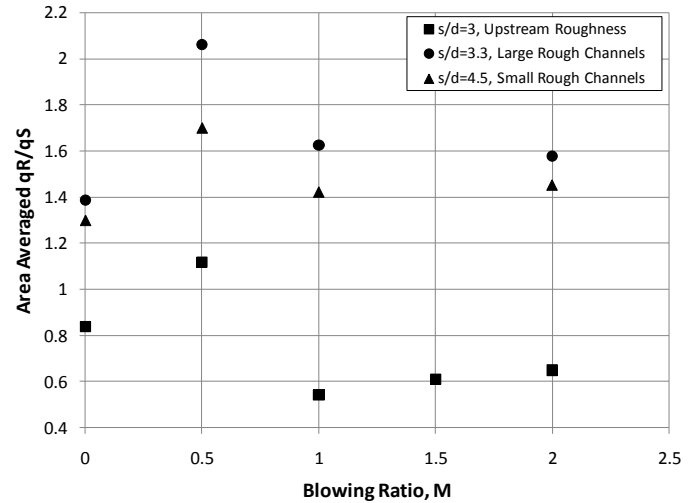


Figure 11: Area-averaged rough-to-smooth heat flux ratio vs. M ($0.5 < x/d < 7$). Comparison at constant blowing ratio.

Since deposits form during service (i.e. after the decision has already been made to configure the turbine vane with film cooling holes), perhaps a more useful comparison is the heat flux with deposit compared to the smooth surface heat flux at the same blowing ratio. Using the same methodology used to derive Eq. (1), this rough-to-smooth heat flux ratio can be developed as shown below:

$$\frac{q_R}{q_S} = \frac{h_R (T_{fR} - T_w)}{h_S (T_{fS} - T_w)} = \frac{h_R \left\{ 1 - \frac{\eta_R}{\Phi} \right\}}{h_S \left\{ 1 - \frac{\eta_S}{\Phi} \right\}} \quad (3)$$

In Eq. (3) it is assumed that T_∞ , T_c , and T_w are identical for both the smooth and deposit cases ($\Phi = 0.6$). This ratio is plotted in Fig. 11 vs. blowing ratio. Note that for $M=0$, $q_R/q_S = h_R/h_S$ (from Fig. 9) identically since η_R and $\eta_S = 0$. Here again the data indicate that deposits increase the heat load (in some cases up to 100%), except for the case of upstream roughness. For the $s/d=3.3$ & 4.5 cases, the increased heat flux is commensurate with the size of the deposit roughness.

Even with the deposit topologies that extend downstream, if the deposits are confined to the region between the holes –

the net effect on heat flux is significantly lower than represented in Fig. 11 due to the insulating properties of the deposit. For example, Fig. 12 shows a contour map of h_R/h_{R0} for the $s/d=4.5$ panel with $M=1$. The regions of elevated heat transfer coefficient correspond to the regions with large deposits [see Fig. 2(c)]. From Fig. 6(c), this is also a region of low η . Conversely, the regions directly downstream of the film hole have both low heat transfer coefficient and high η . Since the elevated h_R is over the deposit peaks which have a finite vertical extent above the smooth surface, the “effective” convection coefficient to the underlying smooth surface should also account for the deposit k/t in series with h_R . A simple 1D heat flow analysis yields

$$h_{R,eff} = \frac{(h_R)(k/t)}{(h_R + k/t)} \quad (4)$$

which for $h_R \gg k/t$ becomes k/t (k is the thermal conductivity of the plastic and t is the local deposit height). For the $s/d=4.5$ panel shown in Fig. 12 ($M=1$), the area-averaged $h_{R,eff}/h_R = 0.75$, or a 25% reduction in the actual heat flux due to the added insulation of the deposit peaks. This would reduce the area-averaged q_R/q_S from 1.42 (in Fig. 11) to 1.07. A similar analysis for the $s/d=3.35$ panel at $M=1$ yields a $h_{R,eff}/h_R$ correction of 0.50, thus reducing the area-averaged q_R/q_S from 1.62 (in Fig. 11) to 0.81. In this case, film cooling is once again beneficial since the regions of high cooling effectiveness have only small deposits and correspondingly low convective heat transfer coefficients. For actual turbine deposits, the magnitude of this insulating effect will depend on the thermal conductivity of the deposit. Most deposits are metal oxides with lower conductivities than typical superalloys, though the actual deposit conductivity is difficult to measure due to its unknown void fraction and fragile structure.

CONCLUSIONS

Accelerated deposits were accumulated on 3 turbine coupons with film cooling. Scaled plastic models of the deposit formations were subsequently used in a low-speed wind tunnel to measure film cooling effectiveness and heat transfer coefficients. Based on the results presented in this study, the following conclusions are offered:

- 1) For roughness located primarily upstream of the film holes, area averaged heat flux in the region up to $x/d=7$ from the film holes is lower with the deposit than without. This is due to the “effective ramp” produced by the upstream deposit, providing a separation cavity for the film cooling to reside in.
- 2) When roughness forms downstream of film holes, it is found primarily between the film holes. This provides an effective smooth channel or “furrow” for the coolant to reside in. Heat transfer levels are correspondingly lower in this smooth channel and effectiveness levels are significantly higher. Due to the insulating effect of the deposits between the film cooling “channels”, the effective heat flux to the underlying smooth surface is significantly reduced even though the calculated rough-surface heat transfer coefficients are higher. It is of note that these “furrowed” deposit structures are particularly relevant since they have been observed on actual turbine hardware as reported by Bons et al. [6]

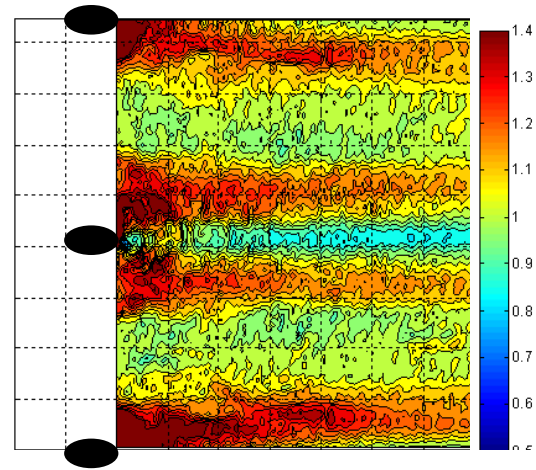


Figure 12: Contour plot of h_R/h_{R0} for $s/d=4.5$, $M=1$ ($0.5 < x/d < 7$, $-4.5 < y/d < 4.5$). Flow is left to right.

ACKNOWLEDGMENTS

Various individuals provided invaluable support to this research effort. The authors would particularly like to thank Dr. Tom Taylor of Praxair Surface Technologies and Dr. Michael Scheurlen from Siemens and Dr. Ron Bunker from GE who generously donated coupon specimens for this study. Thanks also to Shay Pontsler for lending his particular expertise to the construction of the wind tunnel. This work was partially sponsored by a grant the US Department of Energy – National Energy Technology Laboratory through a cooperative agreement with the South Carolina Institute for Energy Studies at Clemson University. The views expressed in this article are those of the authors and do not reflect the official policy or position of the Department of Energy or U.S. Government.

REFERENCES

- [1] Borom, Marcus P., Johnson, Curtis A., and Peluso, Louis A., 1996, “Role of environmental deposits and operating surface temperature in spallation of air plasma sprayed thermal barrier coatings,” *Surface and Coatings Technology* 86-87, pp116-126.
- [2] Wenglarz, R.A., and Fox, R.G. Jr., 1990, “Physical Aspects of Deposition From Coal-Water Fuels Under Gas Turbine Conditions”, *Journal of Engineering for Gas Turbines and Power*, Jan 1990, pp. 9-14.
- [3] Tarada, F. and Suzuki, M., 1993, “External Heat Transfer Enhancement to Turbine Blading due to Surface Roughness,” presented at ASME IGTI in Cincinnati OH, May 1993, ASME Paper 93-GT-74.
- [4] Bons, J. P., 2002, “St and C_f Augmentation for Real Turbine Roughness with Elevated Freestream Turbulence,” *Transactions of the ASME*, vol. 124, OCT 2002, pgs 632-644.
- [5] Kim, J., Dunn, M.G., and Baran, A.J. et al, 1993, “Deposition of Volcanic Materials in the Hot Sections of Two Gas Turbine Engines,” *J. Engr. Gas Turbines & Power* vol. 115, Jul 1993, pp 641-651.
- [6] Bons, J.P., Taylor, R., McClain, S., and Rivir, R.B., 2001, “The Many Faces of Turbine Surface Roughness,” *ASME Journal of Turbomachinery*, Vol. 123, Oct. 2001, pp. 739-748.

- [7] Barlow, D. N., and Kim, Y. W., 1995, "Effect of Surface Roughness on Local Heat Transfer and Film Cooling Effectiveness," *Proceedings of ASME TURBOEXPO 1995*, ASME Paper No. 95-GT-14.
- [8] Rutledge, J. L., Robertson, D., and Bogard, D. G., 2006, "Degradation of Film Cooling Performance On a Turbine Vane Suction Side Due To Surface Roughness," *Journal of Turbomachinery*, Vol. 128, July 2006, pp. 547-554.
- [9] Goldstein, R. J., Eckert, E. R. G., Chiang, H. D., and Elovic, E., 1985, "Effect of Surface Roughness on Film Cooling Performance," *Journal of Engineering for Gas Turbines and Power*, Vol. 107, January 1985, pp. 111-116.
- [10] Bogard, D., Snook, D., and Kohli, A., 2003, "Rough Surface Effects on Film Cooling of the Suction Side Surface of a Turbine Vane," *The 2003 ASME IMECE Conference*, 2003. Paper No. 2003-42061.
- [11] Cardwell, N. D., Sundaram, N., and Thole, K. A., 2006, "Effects of Mid-Passage Gap, Endwall Misalignment and Roughness on Endwall Film-Cooling," *Journal of Turbomachinery*, Vol. 128, Jan. 2006, pp. 62-70.
- [12] Demling, P., and Bogard, D. G., 2006, "The Effects of Obstructions on Film Cooling Effectiveness on the Suction Side of a Gas Turbine Vane," *Proceedings of ASME Turbo Expo 2006: Power for Land, Sea and Air*, GT2006-90577.
- [13] Somawardhana, R. and Bogard, D.G., 2007, "Effects of Surface Roughness and Near Hole Obstructions on Film Cooling Effectiveness," *Proceedings of ASME Turbo Expo 2007*, ASME Paper No. GT2007- 28004.
- [14] Sundaram, N. and Thole, K. A., 2006, "Effects of Surface Deposition, Hole Blockage, and TBC Spallation on Vane Endwall Film-Cooling," *Proceedings of ASME Turbo Expo 2006: Power for Land, Sea and Air*, GT2006-90379
- [15] Jensen, J. W., Squire, S. W., and Bons, J. P., 2005, "Simulated Land-Based Turbine Deposits Generated in an Accelerated Deposition Facility," *ASME J. Turbomach.* vol. 127, JULY 2005, pgs 462-470.
- [16] Crosby, J., Lewis, S., Ai, W., Bons, J.P., and Fletcher, T.H., 2008, "Effects of Temperature and Particle Size on Deposition in Land Based Turbines," *ASME Journal of Engineering for Gas Turbines and Power*, Sept. 2008, Volume 130, Issue 5, 051503.
- [17] Antonia, R.A., and Luxton, R.E., 1971, The Response of a Turbulent Boundary Layer to a Step Change in Surface Roughness. Part 1: Smooth to Rough," *Journal of Fluid Mechanics*, Vol. 48, pp. 721-726.
- [18] Bons, J.P., Wammack, J.E., Crosby, J., Fletcher, D.H., and Fletcher, T.H., 2008, "Evolution of Surface Deposits on a High Pressure Turbine Blade, Part 2: Convective Heat Transfer," *ASME Journal of Turbomachinery*, Apr. 2008, Vol. 130, 021021.
- [19] Ekkad, S.V., Zapata, D., and Han, J.C., 1997, "Film Effectiveness over a Flat Surface with Air and CO₂ Injection through Compound Angle Holes using a Transient Liquid Crystal Image Method," *ASME Journal of Turbomachinery*, Jul. 1997, Vol. 119, pp. 587-593.
- [20] Schultz, D.L. and Jones, T.V., 1973, "Heat-transfer Measurements in Short-duration Hypersonic Facilities," *Advisory Group for Aerospace Research and Development*, No. 165, NATO.
- [21] Bons, J.P., 2009, "Transient Method for Convective Heat Transfer Measurement with Lateral Conduction, Part 1: Analytical Development for Generic Rough Surfaces," *ASME J of Heat Transfer*, Jan 2009.
- [22] Bons, J.P., Fletcher, D., and Borchert, B., 2009, "Transient Method for Convective Heat Transfer Measurement with Lateral Conduction, Part 2: Experimental Application to an Isolated Bump," *ASME J of Heat Transfer*, Jan 2009.
- [23] Brown, A., and Saluja, C.L., 1979, "Film Cooling from a Single Hole and Row of Holes of Variable Pitch to Diameter Ratio," *Int'l J. Heat Mass Transfer*, Vol. 22, pp. 525-533.
- [24] Na, S., and Shih, T. I-P., 2006, "Increasing Adiabatic Film Effectiveness by Using an Upstream Ramp," *Proceedings of ASME Turbo Expo 2006: Power for Land, Sea and Air*, GT2006-91163.
- [25] Barigozzi, G., Franchini, G., and Perichizzi, A., 2007, "The Effect of an Upstream Ramp on Cylindrical and Fan-Shaped Hole Film-Cooling – Part II: Adiabatic Effectiveness Results," *Proceedings of ASME Turbo Expo 2007: Power for Land, Sea and Air*, GT2007-27079.